Defect-Detriment to Graphene Strength Is Concealed by Local Probe: The Topological and Geometrical Effects

Zhigong Song,[†] Vasilii I. Artyukhov,[‡] Jian Wu,[†] Boris I. Yakobson,[*,‡] and Zhiping Xu[*,†]

[†]Applied Mechanics Laboratory, Department of Engineering Mechanics and Center for Nano and Micro Mechanics, Tsinghua University, Beijing 100084, China and [‡]Department of Materials Science and NanoEngineering, Department of Chemistry, and the Richard E. Smalley Institute for Nanoscale Science and Technology, Rice University, Houston, Texas 77005, United States

ABSTRACT Defects in solids commonly limit mechanical performance of materials by reducing their rigidity and strength. However, topological defects also induce a prominent geometrical effect in addition to local stress buildup, which is especially pronounced in two-dimensional crystals. These dual roles of defects modulate mechanical responses of the material under local and global probes in very different ways. We demonstrate through atomistic simulations and theoretical analysis that local response of two-dimensional crystals can even be stiffened and strengthened by topological defects as the structure under indentation features a positive Gaussian curvature, while softened and weakened mechanical responses are measured at locations with negative Gaussian curvatures. These findings shed lights on mechanical characterization of two-dimensional materials in general. The geometrical effect of topological defects also adds a new dimension to material design, in the scenario of geometrical and topological engineering.

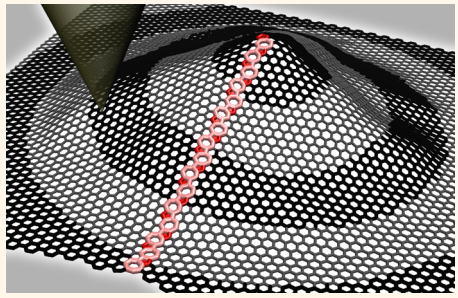

KEYWORDS: graphene · nanoindentation · mechanical properties · material strength · topological effect · geometrical effect

Topological defects (TDs, *e.g.*, dislocations, disclinations) in crystals break the translational invariance of lattice symmetry and alter a vast number of material properties, including mechanical strength, as well as thermal and electronic transport.[1−6] On the basis of in-plane stress/strain theories of elasticity, lattice distortion (prestrain) and stress buildup created by these imperfections can be well formulated except for a core region spanning a few lattice constants, where divergence appears.[7] However, this two-dimensional (2D) theory breaks down in three-dimensional space. Realistic atom-thick sheets such as graphene and polymeric membranes usually display geometrical distortion away from planarity that releases the in-plane stress induced by TDs. For example, a +60° wedge disclination in hexagonal or triangular crystals is 5-fold coordinated and leads to warping with a positive Gaussian curvature K, while a 7-fold coordinated −60° disclination results in distorted geometry with a negative K. Consequently, 2D crystals with TDs that are usually immobile at room temperature are nondevelopable membranes with built-in prestrain.[8] This distinct nature implies renormalization of their physical properties, as widely exemplified in nature and engineering.

Graphene is an excellent illustrative example of 2D crystalline membrane with hexagonal lattice, where TDs arise naturally due to the topological requirement for closed nanostructures or as imperfections formed during the growth stage.[9,10] In single-crystalline graphene, strong covalent C−C bonds yields excellent mechanical properties such as a tensile stiffness of 1 TPa, and an ideal strength of 120 GPa.[11] However, the presence of defects, for instance TDs in grain boundaries (GBs), poses a critical question upon their effects on mechanical performance of graphene membrane, which has not been satisfactorily addressed.[4,5,12−14] The strength of a polycrystalline graphene is not well-defined, as

* Address correspondence to xuzp@tsinghua.edu.cn, biy@rice.edu.

Received for review September 28, 2014 and accepted December 8, 2014.

Published online December 08, 2014
10.1021/nn505510r

one needs to know the "history" of graphene to compute the joint mechanical equilibrium of all its grains.[9] However, various experimental conditions produce different structures in terms of grain size, shape and even degree of "stitching" of grain boundaries.[15−17] Moreover, as a 2D membrane, graphene permits local measurements of strength that are widely pursued in recent experiments,[11,15−17] but the result of such a measurement depends on where and how it is performed. In contrast, in-plane tests are more relevant to practical applications and commonly used in atomistic simulations,[4,5,13] which measure the global strength of 2D material.

In view of the disagreement between recent experimental and simulation work, some clarifications on the local and global strength measurements are urged. First, the structure of GB depends on the synthesis conditions. And second, the strength depends on where and how it is measured. In this work, we explore this problem by considering both roles of TDs in building up local stress field and distorting the planar structure of graphene. Mechanical responses under both local (nanoindentation) and global (in-plane tension) loading conditions are characterized. We find that, the local response is governed by the lattice under indenter, in contrast to the global mechanical performance quantified by in-plane tensile tests. Moreover, geometrical effects from out-of-plane distortion induced by TDs play a signature role in defining the local response, and surprisingly, with a conic shape, the local mechanical response of graphene containing TDs could be even stiffer and stronger than the pristine membrane. The elucidated mechanisms for these phenomena offer new understandings for the correlation between structural defects at atomistic scale and overall mechanical performance of 2D materials.

RESULTS AND DISCUSSION

To quantify mechanical performance of graphene under local and global probes, we carry out classical molecular dynamics (MD) simulations based on the adaptive intermolecular reactive empirical bond-order (AIREBO) potential (see Methods for more details).[18] We explore both pristine and polycrystalline graphene under nanoindentation or equibiaxial in-plane tensile loads. For polycrystalline graphene, we focus on TDs in GBs only. In chemical vapor deposition (CVD) grown graphene, TDs include pentagon-heptagon (5|7) pairs that can be considered as dislocations or disclination pairs, as well as octagons, vacancies, and others that are identified less frequently.[9,17,19,20] Paired 5|7 defects have been observed in tilt GBs and are reported to induce polar and high-amplitude stress buildup in graphene (~56.83 GPa).[9,17] According to the 2D edge dislocation theory, local stress buildup scales as $\sim 1/r$ at a distance r from the defect core, and thus a pileup of 5|7 dislocations leads to stress accumulation.[4,5] As a result, a finite-length (l) GB with 5|7 pairs yields a tensile (compressive) stress buildup $\sigma_b \sim \log l$ at its end terminated with a heptagon (pentagon) and reduces the global strength measured under in-plane loads by an amplitude of the tensile stress buildup σ_b (the pseudo-Hall−Petch effect).[5]

The local mechanical response is probed by simulating nanoindentation tests. A graphene sheet is deposited to an adhesive porous substrate with the pore diameter $2R$ = 11 nm (Figure 1). The indenter is simulated by a spherical particle (the diameter D = 2 nm) placed on top of the GBs, interacting with the carbon atoms in graphene through a force of magnitude $\sim k(r - D/2)^2$. Here the force constant is set to k = 10 eV Å^{-3} that is confirmed to be stiff enough to exclude dynamical effects in the measurement, and r is the distance from the atom to the center of the indenter. As shown in Figure 1a, two types of straight GBs are first explored, including the armchair-oriented GB (aGB) and zigzag-oriented GB (zGB) that correspond to tilt angles of 28.7° and 21.7°, respectively.[13] Graphene with straight GBs across the membrane, *i.e.*, without terminations in the membrane, is relatively flat, with out-of-plane displacement below 0.3 nm. We measure local fracture force of the membrane by the indentation force at fracture. Our simulation results show that when the indenter is pressed down toward the center of membrane, the local fracture forces f_{GB} are 51.92 and 43.95 nN for aGB and zGB, showing reductions of 14.03 and 27.22% from the value for a pristine graphene (f_0 = 60.39 nN). For small deviations the fracture force f can be converted to the two-dimensional strength $\sigma_{2D}t$ following the relation $\sigma_{2D}t = (Ytf/4\pi R)^{1/2}$ for thin clamped, linear elastic circular membrane,[11,21] where Yt is the 2D Young's modulus of graphene with thickness of t, and R is the tip radius of indenter. However, due to the structural distortion and nonlinearity arising, the reliability of this correspondence is weakened and may fail under high loads. So we use the values of fracture force for our following discussions. In a second set of simulations, we consider V-shaped GBs with an angle of $2\pi/3$ (Figure 1b), the fracture forces for aGB and zGB are 51.89 and 43.48 nN, with reductions from the ideal strength by 14.08 and 28%. These results show consistence with recent experimentally measured reduction in the range of 20−40%.[16,17] Our simulation results show that the fracture of polycrystalline graphene nucleates from the lattice under indenter, by breaking C−C bonds shared by neighboring heptagon and hexagon. After this critical point, the crack propagates, resulting in a fracture pattern along the radial directions, at the location with tensile prestrain.[5,9] The same phenomena are observed for both straight and V-shape GBs.

Tensile stress buildup from dislocation pileups in the GBs could lead to prominent strength reduction under uniform uniaxial or equibiaxial in-plane loads.[5]

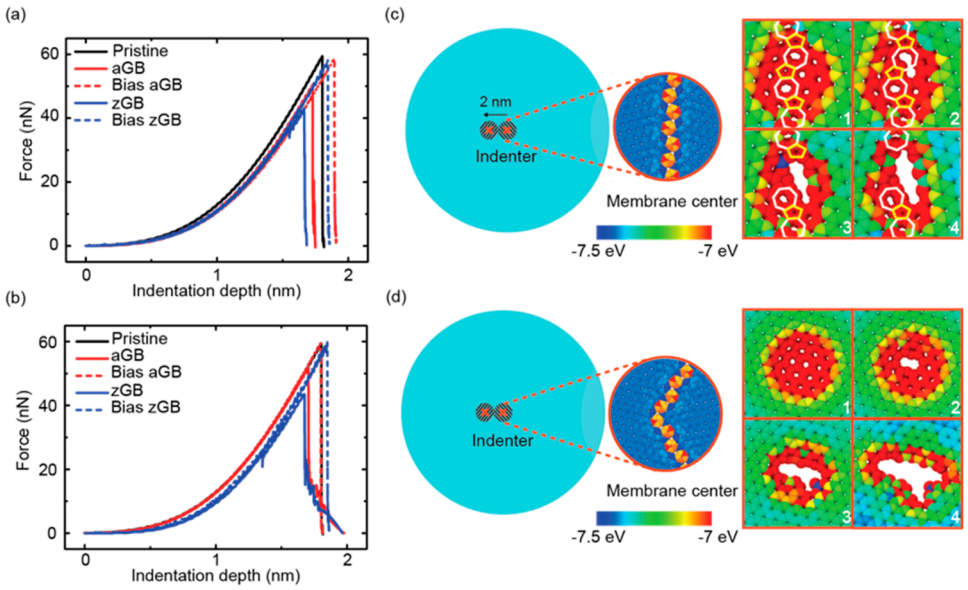

Figure 1. Local strength of graphene with GBs probed by simulated nanoindentation tests. (a) and (b) show the indentation force-depth relations for graphene membranes with straight and V-shape GBs. The atomic structures of GBs in the center of supported polycrystalline membrane and the fracture patterns are plotted in panels (c) and (d), respectively. Nanoindentation is carried out with tip placed in the center or membrane or with an offset of 2 nm. Numbers in panels (c) and (d) indicate the sequence in the fracture process. Colors in panel (c) and (d) depict the potential energy per atom, which will be used in following figures as well.

According to our discussion above, this reduction may not be detected under nanoindentation with the probe displaced away from the buildup. To verify this argument, we further carry out nanoindentation tests by shifting the tip of indenter laterally from the center of graphene membrane by the size of indenter, *i.e.*, 2 nm (see Figure 1c and 1d for illustration). The results show that the intrinsic strength of pristine graphene is recovered with the same GBs across the membrane as explained before, with measured amplitudes for the fracture force as 60.11 and 59.82 nN for straight aGB and zGB, and 59.69 and 59.90 nN for V-shape aGB and zGB, respectively. As in nanoindentation tests for a membrane, the in-plane tensile stress decreases inversely with distance from the indenter tip,[22] and thus the stress under the tip at rupture describes local strength. This sensitivity of measured indentation fracture force to the position of indenter tip may explain the diverse values reported in the literature.[11,15,16,23]

To further illustrate the point that the strength depends on both the lattice structure and where it is measured, we perform indentation tests for graphene membranes supported on a nanopore with semi-infinite and finite GBs where terminations are present. While a GB terminating in the middle of lattice may appear unlikely to form by itself, such structures could be induced by substrate curvature.[24] The results summarized in Figure 2 clearly show nonplanar geometrical distortion. We first measure the mechanical response at a certain distance from semi-infinite GBs that originate from the supported side in contact with the substrate and ending with a pentagon. Nanoindentation test is performed at the center of membrane and the fracture force is measured as a function of the length of GB l, which shows a peak (68.69 nN for aGB, 77.01 nN for zGB) when the end of GBs is located in the center of membrane where the indenter tip is placed (l = 5.57 and 5.10 nm for aGB and zGB, respectively). Remarkably, this fracture force is 13.74% (aGB) or 27.52% (zGB) *higher* than that measured for pristine graphene membrane. This unexpected observation can be explained as a geometrical effect from the conical membrane shape (Figure 2b and 2c) formed due to the presence of pentagon, which is a positive disclination in the hexagonal lattice.[9] To obtain a theoretical description of the mechanism, we simplify the situation into a conical membrane experiencing an indentation force f at the center (Figure 3). The stress distribution in the membrane can be separately determined in two regions, including a conical part free of normal load and a spherical part conformed to the spherical indenter (~1 nm). Arguments can then be made based on axial equilibrium in the noncontact part. At position r measured laterally from the center of membrane, the meridional stress $\sigma_m(r)$ can be related to f as $f = \sigma_m t 2\pi r \sin \varphi$, where t is the thickness of membrane thickness and $\alpha = \pi - 2\varphi$ is the conical angle. As a result, with the same indentation force applied, the amplitude of σ_m decreases as the conical angle decreases, or the height of the cone d_0 increases. By assuming linear in-plane elastic response of graphene, one can see that the effective stiffness $k = \partial f/\partial d$ increases with the cone height d_0 as $k = 2(\cos \varphi) d_0/[D \ln(2R/D \sin \varphi)]$. While under the indenter tip, σ_m increases and circumferential stress arises due to the presence of pressure from indentation. As a result,

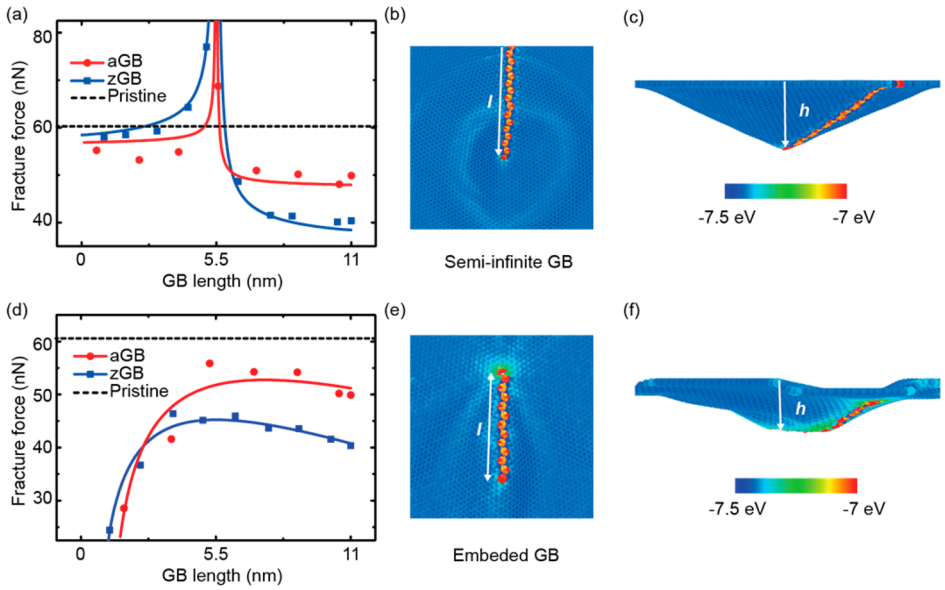

Figure 2. Indentation tests on (a,b,c) semi-infinite and (d,e,f) embedded GBs. The measured fracture force shows significant length-dependence, which arises from a combined effect from the tensile stress buildup in the heptagons and distorted membrane geometry (c,f). Dots and lines are results from MD simulations and analytical fittings, respectively.

fracture in the membrane tends to nucleate under the tip and the fracture force increases with d.

When the indentation is applied far away from the tip of semi-infinite GBs, the graphene lattice under the tip is perfect and thus the fracture force measured is close to that of pristine graphene. While for GBs with length close to the diameter of supporting pore, the measured strength reaches the value for straight GBs accordingly. Between these two limits, the local strength of membrane center can be calculated by incorporating effects from both stress buildup from dislocation pileup[5] and the conic shape. On the basis of our analysis above, the indentation fracture force is $f = [A_1 + B_1 \log_{10} l/(R - l)] \times lR/(2R - l) + f_0$ for $l > R$, and $f = [A_1 + B_1 \log_{10}(2R - l)]/(l - R)] \times R(2R - l)/l + f_{GB}$ for $l < R$, where f_0 and f_{GB} are fracture forces for pristine graphene and graphene with infinite GBs (see Supporting Information for details). Our simulation results can be well captured by fitting the theoretical predictions through parameters A_1 and B_1. The semi-infinite GB terminated by a heptagon is also investigated. However, the out-of-plane distortion does not allow the graphene membrane to be well adhered to the substrate and the structure becomes mechanically unstable due to the presence of high tensile stress at its end.[5] This makes quantitative discussion on the strength of semi-infinite GBs with heptagon termination unfeasible.

For the embedded GB with 5|7 pairs shown in Figure 2e and 2f, two ends are terminated by the pentagon and heptagon, respectively. The pretension built up at the bond between heptagon and hexagon leads to significant reduction of the measured strength. As the length of GB l increases and the leading heptagon moves away from the position of indentation, the measured strength increases to a peak with the aforementioned geometrical effect. Beyond this length, the amplitude of out-of-plane distortion is reduced and the fracture force decays to the value of a straight GB across the whole membrane. These results can also be well fitted to $f = [A_2 + 1/(l - l_c) + 1/l + 1/(l + l_c)](B_2 l + C_2)$ by tuning parameters A_2, B_2 and C_2, where the terms $1/(l - l_c)$, $1/l$ and $1/(l + l_c)$ arise from stress buildups and l_c is the contact length between indenter and graphene (see Supporting Information for details). Embedded GBs with two ends terminated by pentagons or heptagons only are also investigated, but the results show irregular dependence on the length of GB due to the magnified warping of the membrane.

To further explore the combined effect of stress buildup and geometrical distortion from 5|7 dislocations, we construct a set of polycrystalline graphene sheets containing triple-GB junctions (Figure 3a), which are usually the weakest point under mechanical loading.[5] Here the surface roughness with amplitude of a few nanometers is consistent with experimental evidence.[15] The results from indentation tests are summarized Figure 3b–e, which display distinct dependence of the stiffness and strength on the membrane morphology at rest. Specifically, we observe a positive correlation between the indentation strength, stiffness and ultimate indentation depth before fracture $d = d_0 + \Delta d$, where d_0 is the depth due to the presence of TDs and Δd is the displacement induced by the indentation force. This observation is consistent with our previous discussion on the geometrical effect and the f–d dependence. From the simulation results, we find that for junction with a pentagon/heptagon at the indentation position, the fracture force is enhanced/reduced. In contrast to the stiffening effect

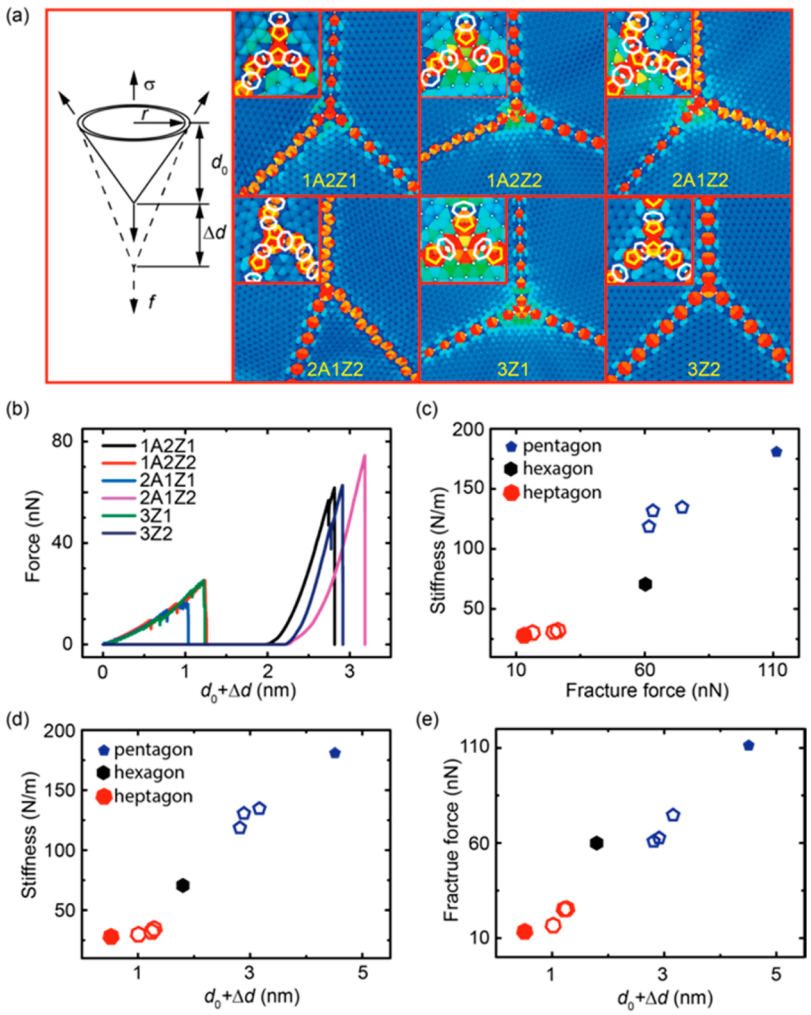

Figure 3. Nanoindentation tests on triple-GB junctions. (a) The atomic structures show distinct out-of-plane buckling morphology. (b) and (c), the measured indentation strength shows significant dependence of the membrane morphology, as indicated by the correlation between fracture force, stiffness and the vertical position of indenter $d = d_0 + \Delta d$ (d,e).

from warping with positive Gaussian curvature where the membrane is stretched, the wrinkles formed around heptagons are softened due to the negligible bending rigidity of graphene. This softened elastic response was also observed in nanoindentation tests for graphene with out-of-plane rippling created during growth and transfer processes, as the force required to flatten out the ripples is considerably smaller than the force needed to cause in-plane stretch.[15] The strength and stiffness of the membrane gradually changes from the values for a single pentagon/heptagon under indentation, approaching the value for pristine graphene with a hexagon there. These results clearly indicate the combined effect of local lattice imperfections and geometry in defining the indentation strength of graphene with TDs.

In polycrystalline graphene grown by CVD, GBs form when neighboring flakes meet up.[9,17,19,20,24] The single-crystalline domains are usually much larger than the contact area between graphene and the indenter, and thus the GBs may not necessarily be detected under local probes. A direct conclusion from our findings is that the fracture force, and stiffness measured in nanoindentation tests quantify only local responses of 2D materials, and may not capture the global material performance concerned in practical applications, such as nanoeletromechanical devices and nanocomposites, where in-plane tensile loads are imposed. Additional information about the type and distribution of defects and morphological warping are required for rigorous discussion on the mechanical properties of graphene with TDs that, however, lacks from recent experimental studies due to the technical challenges,[16,17,25] although the *in situ* tensile tests on precracked bilayer graphene reported recently may eventually be refined to clarify this issue.

This conclusion can be further illustrated by considering a pristine graphene sheet consisting of a hexagonal 5|7 dislocation loop at a distance r from the center of membrane.[26,27] We find that, as shown in Figure 4, the strength measured from nanoindentation and equibiaxial loading tests features contrasting

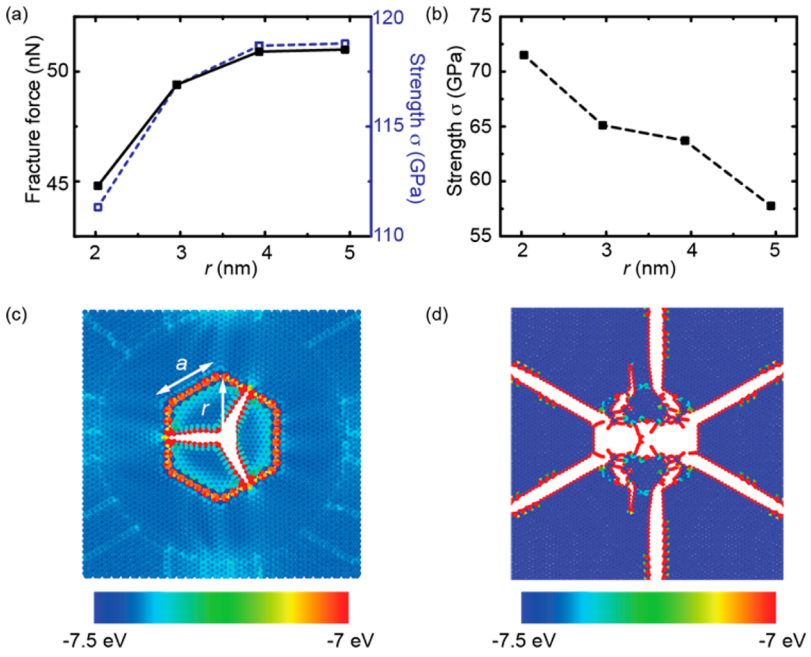

Figure 4. Fracture force (the solid line) and tensile strengths (dash lines) measured for a graphene sheet containing a 5|7 dislocation loop, as measured from (a) nanoindentation and (b) equibiaxial tensile tests. The strength σ in (a) is converted from the fracture force based on the linear elastic membrane model, by assuming the graphene with thickness of 0.34 nm (see text). Panels (c) and (d) show the fracture patterns, which nucleate from the center of membrane and dislocation loop, respectively.

r-dependence. In nanoindentation, the fracture nucleates from the center of membrane under the indentation tip (Figure 4c) and the strength measures the critical indentation force of perfect graphene lattice with perturbation from the dislocation loop around. As the stress induced by the dislocations decays radially from the dislocation, the measured strength increases as the size of defect loop a (= r) increases and approaches the value for pristine graphene. In contrast, in the equibiaxial tensile tests, the strength of the material is defined by the maximum tensile stress buildup in the membrane, which increases with the size of defect loop following the pseudo-Hall–Petch mechanism.[5] As a result, the fracture nucleates from the defects (Figure 4d), and the strength measured decreases with a, in opposite to the indentation test.

CONCLUSION

The dual roles of TDs in GBs in defining the strength of pristine or defected graphene have thus been assessed. The local stress buildup reduces its strength, while local lattice distortion modulates it further under local mechanical probes, in contrast to the situation where in-plane loads are imposed globally. These findings elucidate the possible mechanisms featured by reported simulation and experimental results, and raise the question of how the fracture force measured by nanoindentation could be mapped to strength of the material under tensile loading conditions that are more common in practical applications.

Moreover, these findings also imply that mechanical properties of 2D materials could be tuned to a large extent by simply implanting topological defects that result in stress localization and geometrical distortion. For example, carbon nanocones could be used as extremely sharp probes in atomic imaging, and hourglass-shape nanochannels hold promises in optimal hydrodynamic transport.[28−31] Material design following this approach could be achieved by growing graphene on a curved substrate[24] and then the adhesion between the membrane and substrate could force the growth to create topological defects compatible with the substrate geometry. One could also engineer the structure by after-growth treatments such as irradiation and functionalization. Structural relaxation could then anneal the defective structure into a lattice with topological defects or geometrical distortion. If the treatment could be rationally controlled with nanoscale spatial precision, geometrical design of these materials will be feasible. These concepts could be extended to other 2D materials.

METHODS

Simulation details: Molecular dynamics (MD) simulations were performed to explore the mechanical responses of graphene using the large-scale atomic/molecular massively parallel simulator (LAMMPS).[32] We used the adaptive intermolecular reactive empirical bond-order (AIREBO) potential energy function that describes the interatomic interaction between carbon atoms.[18] For the parameters in AIREBO potential

functions, the cutoff distance is adjusted to 0.2 nm to avoid the spurious strengthening effect that corresponds to a spurious stress peak after structure failure occurs.[33] As discussed and verified in the literature,[4,5,13,33] this set of potential and parameters offers quantitatively reliable prediction of the mechanical properties of graphitic structures. In our work,[5] we compared the performance of AIREBO potential with both reactive force field (ReaxFF)[34,35] and density functional theory (DFT) based first-principles calculations,[36] which show consistent results. Specifically, for graphene with an embedded Stone–Wales defect (modeled using a supercell containing 50 carbon atoms), the AIREBO-based calculation predicts a formation energy of 5.23 eV, while Perdew–Burke–Ernzerhof (PBE)[37] based DFT calculations using the Vienna *ab initio* package (VASP)[38] predicts 5.26 eV.

The atomic structure of graphene constructed was optimized using a conjugated-gradient algorithm before mechanical tests were performed. The mechanical responses were probed by performing MD simulations at both 0 K (that is, no initial thermalization was performed, but as the simulation proceeds, temperature of the atomic system could rise to a few Kelvin) and 300 K using a Nosé–Hoover thermostat with a damping time constant $\tau_T = 0.1$ ps. The stiffness of graphene is lowered by only 2.2% at 300 K, compared to the value obtained at 0 K (0.9 TPa with the thickness of graphene considered as 0.34 nm). The AIREBO-based MD results for the stress–strain relation shown great consistence with DFT predictions.[5]

In nanoindentation simulations, a virtual substrate is used to support a squared graphene sheet with size of 20 nm. The edges of graphene are fixed during the indentation tests. The loading speed is 1 m/s, and in the tensile tests, strain was applied at a rate of 1 ns^{-1}. Simulations at lower loading rates were also performed to verify that the deformation and fracture behavior are not affected by the dynamical effect. In the tensile tests, the stress is calculated by considering the thickness of graphene as 0.34 nm.

Conflict of Interest: The authors declare no competing financial interest.

Acknowledgment. This work was supported by the National Natural Science Foundation of China through Grant 11222217, 11002079, and the State Key Laboratory of Mechanics and Control of Mechanical Structures (Nanjing University of Aeronautics and Astronautics) through Grant No. MCMS-0414G01. The simulations were performed on the Explorer 100 cluster system of Tsinghua National Laboratory for Information Science and Technology. Work at Rice was supported by the US Air Force Office of Scientific Research Grant FA9550-13-1-0151 and in part by the Office of Naval Research MURI Grant N00014-09-1-1066.

Supporting Information Available: Detailed information on atomic structures of GBs in graphene; mechanical responses of graphene with semi-infinite and embedded GBs under indentation, or tensile tests; fitting parameters for Figure 2; formation energy of finite-length GBs in graphene are provided. This material is available free of charge *via* the Internet at http://pubs.acs.org.

Note Added after ASAP Publication: This paper published ASAP on December 17, 2014. References 3 and 5 were modified and the revised version was reposted on December 19, 2014.

REFERENCES AND NOTES

1. Nelson, D. R. *Defects and Geometry in Condensed Matter Physics*; Cambridge University Press: Cambridge, U.K., 2002.
2. Yazyev, O. V.; Louie, S. G. Electronic Transport in Polycrystalline Graphene. *Nat. Mater.* **2010**, *9*, 806–809.
3. Song, Z.; Xu, Z. Topological defects in two-dimensional crystals: Stress buildup and accumulation. *J. Appl. Mech.* **2014**, *81*, 091004.
4. Wei, Y. J.; Wu, J.; Yin, H.; Shi, X.; Yang, R.; Dresselhaus, M. S. The Nature of Strength Enhancement and Weakening by Pentagon-Heptagon Defects in Graphene. *Nat. Mater.* **2012**, *11*, 759–763.
5. Song, Z.; Artyukhov, V. I.; Yakobson, B. I.; Xu, Z. Pseudo Hall-Petch Strength Reduction in Polycrystalline Graphene. *Nano Lett.* **2013**, *13*, 1829–1833.
6. Wang, Y.; Song, Z.; Xu, Z. Characterizing Phonon Thermal Conduction in Polycrystalline Graphene. *J. Mater. Res.* **2014**, *29*, 362–372.
7. Landau, L. D.; Lifshitz, E. M. *Theory of Elasticity*; Butterworth-Heinemann: Oxford, U.K., 1986.
8. Liu, Y.; Yakobson, B. I. Cones, Pringles, and Grain Boundary Landscapes in Graphene Topology. *Nano Lett.* **2010**, *10*, 2178–2183.
9. Yakobson, B. I.; Ding, F. Observational Geology of Graphene, at the Nanoscale. *ACS Nano* **2011**, *5*, 1569–1574.
10. Banhart, F.; Kotakoski, J.; Krasheninnikov, A. V. Structural Defects in Graphene. *ACS Nano* **2010**, *5*, 26–41.
11. Lee, C.; Wei, X.; Kysar, J. W.; Hone, J. Measurement of the Elastic Properties and Intrinsic Strength of Monolayer Graphene. *Science* **2008**, *321*, 385–388.
12. Malola, S.; Häkkinen, H.; Koskinen, P. Structural, Chemical, and Dynamical Trends in Graphene Grain Boundaries. *Phys. Rev. B: Chem. Matter Mater. Phys.* **2010**, *81*, 165447.
13. Grantab, R.; Shenoy, V. B.; Ruoff, R. S. Anomalous Strength Characteristics of Tilt Grain Boundaries in Graphene. *Science* **2010**, *330*, 946–948.
14. Zhang, T.; Li, X.; Kadkhodaei, S.; Gao, H. Flaw Insensitive Fracture in Nanocrystalline Graphene. *Nano Lett.* **2012**, *12*, 4605–4610.
15. Ruiz-Vargas, C. S.; Zhuang, H. L.; Huang, P. Y.; van der Zande, A. M.; Garg, S.; McEuen, P. L.; Muller, D. A.; Hennig, R. G.; Park, J. Softened Elastic Response and Unzipping in Chemical Vapor Deposition Graphene Membranes. *Nano Lett.* **2011**, *11*, 2259–2263.
16. Lee, G.-H.; Cooper, R. C.; An, S. J.; Lee, S.; van der Zande, A.; Petrone, N.; Hammerberg, A. G.; Lee, C.; Crawford, B.; Oliver, W.; *et al.* High-Strength Chemical-Vapor-Deposited Graphene and Grain Boundaries. *Science* **2013**, *340*, 1073–1076.
17. Rasool, H. I.; Ophus, C.; Klug, W. S.; Zettl, A.; Gimzewski, J. K. Measurement of the Intrinsic Strength of Crystalline and Polycrystalline Graphene. *Nat. Commun.* **2013**, *4*, 2811.
18. Brenner, D. W.; Shenderova, O. A.; Harrison, J. A.; Stuart, S. J.; Ni, B.; Sinnott, S. B. A Second-Generation Reactive Empirical Bond Order (REBO) Potential Energy Expression for Hydrocarbons. *J. Phys.: Condens. Matter* **2002**, *14*, 783–802.
19. Kim, K.; Lee, Z.; Regan, W.; Kisielowski, C.; Crommie, M. F.; Zettl, A. Grain Boundary Mapping in Polycrystalline Graphene. *ACS Nano* **2011**, *5*, 2142–2146.
20. Lahiri, J.; Lin, Y.; Bozkurt, P.; Oleynik, I. I.; Batzill, M. An Extended Defect in Graphene as a Metallic Wire. *Nat. Nano.* **2010**, *5*, 326–329.
21. Bhatia, N. M.; Nachbar, W. Finite Indentation of an Elastic Membrane by a Spherical Indenter. *Int. J. Nonlinear Mech.* **1968**, *3*, 307–324.
22. Begley, M. R.; Mackin, T. J. Spherical Indentation of Freestanding Circular Thin Films in the Membrane Regime. *J. Mech. Phys. Solids* **2004**, *52*, 2005–2023.
23. Huang, P. Y.; Ruiz-Vargas, C. S.; van der Zande, A. M.; Whitney, W. S.; Levendorf, M. P.; Kevek, J. W.; Garg, S.; Alden, J. S.; Hustedt, C. J.; Zhu, Y.; *et al.* Grains and Grain Boundaries in Single-Layer Graphene Atomic Patchwork Quilts. *Nature* **2011**, *469*, 389–392.
24. Bets, K. V.; Artyukhov, V. I.; Yakobson, B. I. Kinetically determined shapes of grain boundaries in CVD graphene. *arXiv:1412.4323*, **2014**.
25. Kim, K.; Artyukhov, V. I.; Regan, W.; Liu, Y.; Crommie, M. F.; Yakobson, B. I.; Zettl, A. Ripping Graphene: Preferred Directions. *Nano Lett.* **2011**, *12*, 293–297.
26. Cockayne, E.; Rutter, G. M.; Guisinger, N. P.; Crain, J. N.; First, P. N.; Stroscio, J. A. Grain Boundary Loops in Graphene. *Phys. Rev. B: Chem. Matter Mater. Phys.* **2011**, *83*, 195425.
27. Robertson, A. W.; Allen, C. S.; Wu, Y. A.; He, K.; Olivier, J.; Neethling, J.; Kirkland, A. I.; Warner, J. H. Spatial Control of Defect Creation in Graphene at the Nanoscale. *Nat. Commun.* **2012**, *3*, 1144.
28. Gravelle, S.; Joly, L.; Detcheverry, F.; Ybert, C.; Cottin-Bizonne, C.; Bocquet, L. Optimizing Water Permeability through the Hourglass Shape of Aquaporins. *Proc. Natl. Acad. Sci. U. S. A.* **2013**, *110*, 16367–16372.

29. Wales, D. J. Chemistry, Geometry, and Defects in Two Dimensions. *ACS Nano* **2014**, *8*, 1081–1085.
30. Pacheco Sanjuan, A. A.; Mehboudi, M.; Harriss, E. O.; Terrones, H.; Barraza-Lopez, S. Quantitative Chemistry and the Discrete Geometry of Conformal Atom-Thin Crystals. *ACS Nano* **2014**, *8*, 1136–1146.
31. Zhang, T.; Li, X.; Gao, H. Defects Controlled Wrinkling and Topological Design in Graphene. *J. Mech. Phys. Solids* **2014**, *67*, 2–13.
32. Plimpton, S. Fast Parallel Algorithms for Short-Range Molecular Dynamics. *J. Comput. Phys.* **1995**, *117*, 1–19.
33. Xu, Z. Graphene Nano-Ribbons under Tension. *J. Comp. Theor. Nanosci.* **2009**, *6*, 625–628.
34. van Duin, A. C. T.; Dasgupta, S.; Lorant, F.; Goddard, W. A., III ReaxFF: A Reactive Force Field for Hydrocarbons. *J. Phys. Chem. A* **2001**, *105*, 9396–9409.
35. Sen, D.; Novoselov, K. S.; Reis, P. M.; Buehler, M. J. Tearing Graphene Sheets from Adhesive Substrates Produces Tapered Nanoribbons. *Small* **2010**, *6*, 1108–1116.
36. Liu, Y.; Dobrinsky, A.; Yakobson, B. I. Graphene Edge from Armchair to Zigzag: The Origins of Nanotube Chirality? *Phys. Rev. Lett.* **2010**, *105*, 235502.
37. Perdew, J. P.; Burke, K.; Ernzerhof, M. Generalized Gradient Approximation Made Simple. *Phys. Rev. Lett.* **1996**, *77*, 3865–3868.
38. Kresse, G.; Furthmüller, J. Efficient Iterative Schemes for *Ab Initio* Total-Energy Calculations Using a Plane-Wave Basis Set. *Phys. Rev. B: Chem. Matter Mater. Phys.* **1996**, *54*, 11169–11186.